LAWRENCE
LIVERMORE
NATIONAL
LABORATORY

UCRL-TR-227651

Feasibility of measuring 3He bubble diameter populations in deuterium-tritium ice layers using Mie scattering

N. Izumi

February 1, 2007

This work was performed under the auspices of the U.S. Department of Energy by University of California, Lawrence Livermore National Laboratory under Contract W-7405-Eng-48.

Feasibility of measuring 3He bubble diameter populations in deuterium-tritium ice layers using Mie scattering.

Nobuhiko Izumi

Contents

I. Summary

In this report, I assess the feasibility of using Mie scattering to quantify the diameter distribution of ^{3}He bubbles in DT ice layers. Mie scattering methods are often used for diameter measurements of particulates in emulsions like pigments and ink products. This suggests that similar techniques could be used to measure the distribution of ^{3}He bubbles in DT ice layers, which is important for NIF ICF capsules. To investigate the achievable performance of bubble diameter measurements using Mie scattering, I performed numerical modeling using exact analytical expressions.

Mie scattering is light scattering by spherical particulates which have different refractive indices than their surrounding medium. Mie's theoretical model of this problem applies to diffraction by any number of spheres that are all of the same diameter and composition, provided they are randomly distributed and separated from each other by distances that are large compared to the light scattering wavelength. [1]

When a sample which has particulates of a single radius a (i.e. a monodisperse system) is illuminated by monochromatic and polarized laser light (wavelength λ), the angular distribution of the scattered light has a peak in the forward direction along with several narrow minima. The number and angular directions of the minima are specific to the particle size normalized by the wavelength (a/λ). Therefore it is possible to infer the particle size by measuring the angular distribution of the scattered light. However, when the bubble sizes are distributed in diameter (i.e. a polydisperse system), the angular distribution of the scattered light is given by the linear summation of the scattering from each bubble. Therefore, the dips in the angular profile are smoothed out, and it becomes difficult to infer the diameter distribution from the angular distribution alone in polydisperse systems.

In addition to monochromatic laser illumination, it is also possible to illuminate the samples with white un-polarized light and to observe the spectra of scattered light from one or more directions. Similar to the monochromatic illumination described above, the spectrum of scattered light has narrow dips at specific wavelengths related to the bubble diameter. In polydisperse system, however, the observed spectrum is the sum of scattering light rays from bubbles with various sizes. Therefore, the spectral dips are smoothed out, and it is again difficult to use the dips to measure the bubble size distribution in polydisperse systems.

A well-known variation of the static particle size distribution measurements described above is the dynamic light scattering method. When the scattering centers are undergoing Brownian motion in a liquid matrix, the size of the particles and their speed of diffusion can be related using knowledge of the viscosity of the medium [2]. By measuring temporal fluctuations of the light scattered by particulates and analyzing the self correlation of the signal, it is possible to measure the size distribution of the particulates in polydisperse systems. This technique is applicable to a wide diameter range, even for particles smaller than the light wavelength (down to ~ 10nm). However, the ^{3}He bubbles in DT ice layers do not undergo Brownian motion, and more specifically the relation of bubble size and migration speed is not known. Therefore, dynamic light scattering methods are not easily adaptable to the present application.

Because of these reasons, it will be difficult to measure the population of bubbles using either static or dynamic Mie scattering methods. However, it may still be possible to infer the bubble size distribution by analyzing the spectrum of the scattered light. Qualitatively, light scattering by bubbles can be classified into two different regions, Rayleigh and Mie scattering. The transition between these scattering regimes is characterized by a function of a dimensionless parameter $q = 2\pi\left(a/\lambda^{(I)}\right)$ (bubble radius: a, wavelength of light in surrounding medium: $\lambda^{(I)}$)[†],

(1) Rayleigh scattering, $q < 0.4$
Cross-section $\sigma \sim \lambda^{-4}$ (the reason for a blue sky)
(2) Mie scattering, $0.4 < q < 3$
Cross-section $\sigma \sim$ roughly independent to λ (the reason for a white cloud).

Even in polydisperse systems, this significant spectral transition (from Rayleigh to Mie scattering in the wavelength domain) may be observable. The bubble distribution function could then be inferred by fitting the observed spectrum using a back propagation method.

[†] The notation used in this document follows that of Born and Wolf. A subscript of a shoulder of lambda expresses the wavelength in the media surrounding the bubbles.

II. Background

In NIF ignition experiments, a mixture of deuterium and tritium will be used as fuel. To ignite the fuel, very high temperatures and densities have to be established simultaneously. This requires an implosion with very high spherical symmetry. Any perturbations, such as drive non-uniformities, roughness on the shell surfaces, or imperfections in the DT ice layers, can trigger fluid instabilities that will interfere with the uniformity of the implosion.

Tritium is a radioactive isotope which has a half life of 12.26 years. After beta decay, it converts to ^{3}He. The ^{3}He atoms produced in the DT ice layer migrate in the ice layer by diffusion, and a significant fraction of them reach to the ice-gas boundary and enter the gas region. Therefore, the gas pressure in the shell increases in time due to the increase in ^{3}He pressure. As the ^{3}He atoms migrate, they localize in DT ice imperfections and form bubbles. Since the mass density of the gas in the bubbles is 3 orders of magnitude less than the surrounding ice, the resulting perturbations can trigger fluid instabilities during the implosion. The allowable degree of fluid instability therefore sets a requirement on the presence of ^{3}He bubbles within the ice, and it is important to characterize the ^{3}He bubble density in the DT ice layer in order to determine whether the requirements are satisfied.

Several different techniques have been considered to infer the ^{3}He bubble population:

1) Imaging with x-ray or visible light
2) Scattering or diffraction of VUV/visible light,
3) Magnetic resonance microscopy

For bubbles which have relatively large diameter ($> 0.5\mu$m), imaging with visible or x-ray microscopy is possible. However, due to limited spatial resolution, imaging of bubbles smaller than 0.5 μm is not practical. Even small bubbles can seed mass perturbations if they are not uniformly distributed in the ice layer, and so we need to employ a method which has good sensitivity to bubbles smaller than the resolution limit of imaging systems.

In the last decade, significant progress has been made in the field of magnetic resonance microscopy (MRM). Because MRM directly measures the three dimensional distribution of isotopes, this technique is interesting for application to the measurement of unevenly distributed tritium in DT ice layers. However, the spatial resolution of this technique is still comparable to optical microscopy (~1 μm). Signal-to-noise and contrast will also be low, requiring long scanning times.

This memo assesses the expected performance of bubble size distribution measurements with static Mie scattering, considering both angular distributions and spectral distributions as diagnostics of the bubble size distribution.

III. Modeling of Mie scattering

Fig. 1. sketches the experiment geometry. The refractive indices of the surrounding media n^{I} and the bubble n^{II} are set to 1.2 and 1.0 regardless of the light wavelength. The intensity of the light scattered by Mie scattering is calculated as a function of the deflection angle θ and the light wavelength λ [3].

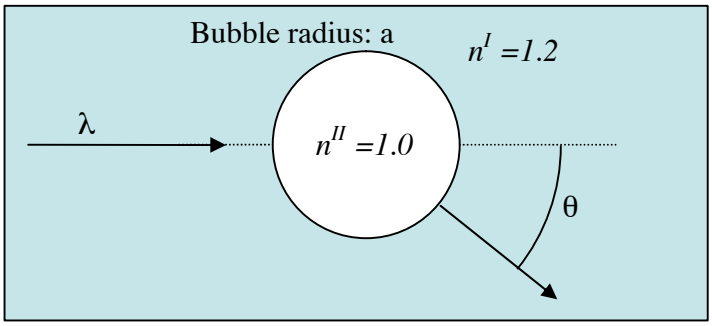

Fig. 1. Schematic diagram of model used in calculation of Mie scattering

$$E_{\theta}^{(S)} = -\frac{1}{k^{(I)}}\frac{\cos\phi}{r}\sum_{l=1}^{\infty}\left[{}^{e}B_l \zeta_l^{(1)'}\left(k^{(I)}r\right)P_l^{(1)'}(\cos\theta)\sin\theta - i\,{}^{m}B_l \zeta_l^{(1)}\left(k^{(I)}r\right)P_l^{(1)}(\cos\theta)\frac{1}{\sin\theta}\right],$$

$$E_{\phi}^{(S)} = -\frac{1}{k^{(I)}}\frac{\sin\phi}{r}\sum_{l=1}^{\infty}\left[{}^{e}B_l \zeta_l^{(1)'}\left(k^{(I)}r\right)P_l^{(1)}(\cos\theta)\frac{1}{\sin\theta} - i\,{}^{m}B_l \zeta_l^{(1)}\left(k^{(I)}r\right)P_l^{(1)'}(\cos\theta)\sin\theta\right],$$

$$H_{\theta}^{(S)} = -\frac{1}{k_2^{(I)}}\frac{\sin\phi}{r}\sum_{l=1}^{\infty}\left[{}^{e}B_l \zeta_l^{(1)}\left(k^{(I)}r\right)P_l^{(1)}(\cos\theta)\frac{1}{\sin\theta} + i\,{}^{m}B_l \zeta_l^{(1)'}\left(k^{(I)}r\right)P_l^{(1)'}(\cos\theta)\sin\theta\right],$$

$$H_{\phi}^{(S)} = -\frac{1}{k_2^{(I)}}\frac{\cos\phi}{r}\sum_{l=1}^{\infty}\left[{}^{e}B_l \zeta_l^{(1)}\left(k^{(I)}r\right)P_l^{(1)'}(\cos\theta)\sin\theta + i\,{}^{m}B_l \zeta_l^{(1)'}\left(k^{(I)}r\right)P_l^{(1)}(\cos\theta)\frac{1}{\sin\theta}\right],$$

where ${}^{e}B_l$ and ${}^{m}B_l$ are complex amplitudes of electric and magnetic partial waves,

$${}^{e}B_l = i^{l+1}\frac{2l+1}{l(l+1)}\bullet\frac{\hat{n}\psi_l'(q)\psi_l(\hat{n}q)-\psi_l(q)\psi_l'(\hat{n}q)}{\hat{n}\zeta_l^{(1)}(q)\psi_l(\hat{n}q)-\zeta_l^{(1)}(q)\psi_l'(\hat{n}q)},$$

$${}^{m}B_l = i^{l+1}\frac{2l+1}{l(l+1)}\bullet\frac{\hat{n}\psi_l(q)\psi_l'(\hat{n}q)-\psi_l'(q)\psi_l(\hat{n}q)}{\hat{n}\zeta_l^{(1)}(q)\psi_l'(\hat{n}q)-\zeta_l^{(1)}{}'(q)\psi_l(\hat{n}q)},$$

ψ(ρ) are ζ(ρ) expressed by Bessel functions and Neumann functions,

$$\psi_l(\rho) = \sqrt{\frac{\pi\rho}{2}}J_{l+\frac{1}{2}}(\rho),$$

$$\chi_l(\rho) = -\sqrt{\frac{\pi\rho}{2}}N_{l+\frac{1}{2}}(\rho),$$

$$\zeta_l^{(1)}(\rho) = \psi_l(\rho) - i\chi_l(\rho).$$

The addition of a prime to the functions ψ(ρ), ζ(ρ) and P(ρ) denotes differentiation with respect to their arguments. The intensity of scattered light which has electric vector along θ and ϕ directions is calculated with the Poynting vector,

$$I_\theta \propto \mathrm{Re}\left(E_\theta^{(S)} \times H_\phi^{(S)*}\right)$$
$$I_\phi \propto \mathrm{Re}\left(E_\phi^{(S)} \times H_\theta^{(S)*}\right).$$

IV. Angular distribution of light scattered by bubbles

Expected angular distribution of uniform-size bubbles (monodisperse systems)

As a first step, the angular distribution of scattered light was calculated for different bubble sizes. As expected, the angular profile of the distribution is determined by the dimensionless parameter $q = 2\pi\left(a/\lambda^{(I)}\right)$. When the void diameter is smaller than the wavelength (a < λ), the angular distribution of the scattered light has less structure and has a broad peak in the forward direction (Rayleigh scattering). When the void diameter is larger than the wavelength (Mie scattering), the angular distribution of the scattered light is forward oriented and has more resonance peaks. Fig. 2 below indicates that,

(1) Light rays scattered by Mie scattering is strongly forward oriented,
(2) Cross section of Mie scattering is strong function of the void diameter.

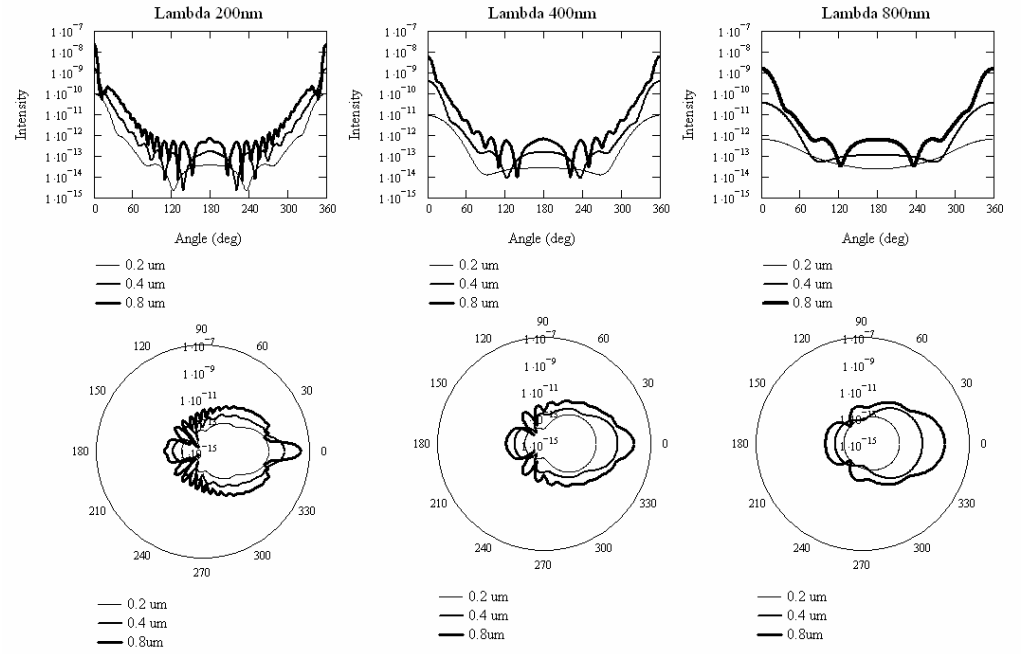

Fig. 2 Angular distribution of light scattered by the void in a dielectric medium. Left: λ (equiv. vacuum) =200nm, Center: λ=400 nm, Right: λ=800 nm.

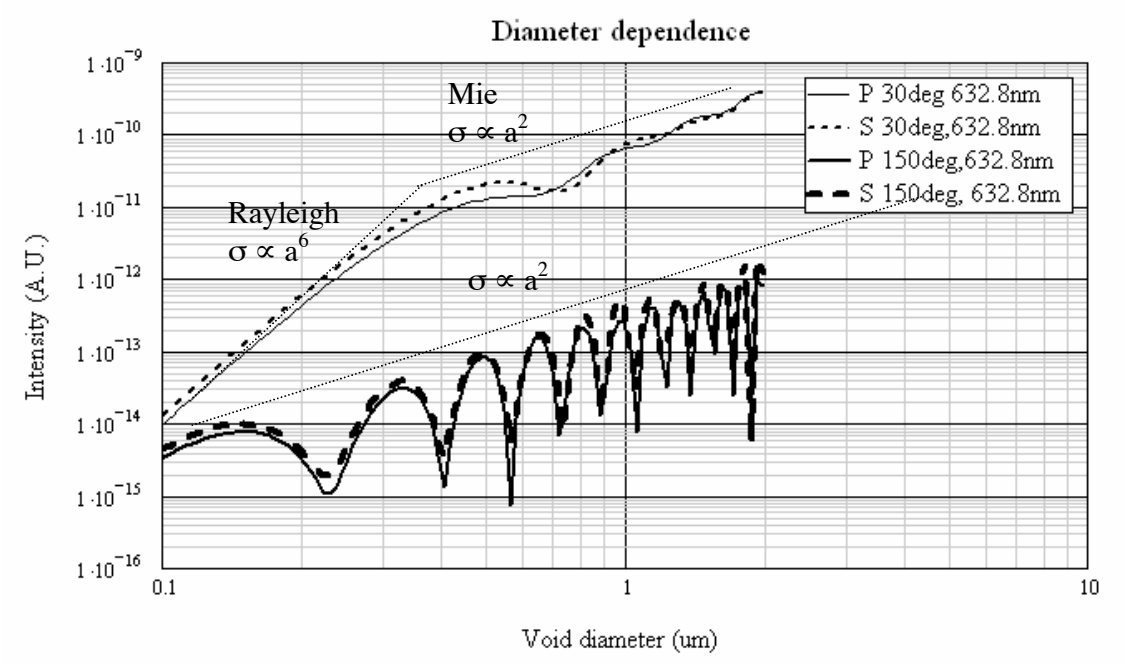

Fig. 3. Intensity of Mie scattering versus void diameter (mono-disperse systems).

Fig. 3 shows the expected signal intensity versus diameter of the bubble. We can conclude that:

(a) Forward Rayleigh scattering ($\theta = 30$deg, $q < 0.4$)

The cross section of forward scattering is a very sensitive function of the void radius ($\sigma \propto a^6$). Therefore the signal observed from the front side is dominated by light scattered by the largest bubbles in the illuminated volume. The strong signal from these large bubbles dominates over the weak signal from smaller bubbles.

(b) Forward Mie scattering ($\theta = 30$deg, $0.4 < q < 3$)

When the bubble diameter is comparable to the wavelength, the cross section of forward scattering ($\theta = 30$ deg.) is proportional to its geometrical cross-section ($\sigma \propto a^2$).

(c) When the scattering angle is large ($\theta = 150$ deg.), the transition point of Rayleigh and Mie scattering moves to the shorter wavelength side. Then, the cross-section is roughly proportional to the geometrical cross-section ($\sigma \propto a^2$).

Expected angular distribution with various bubble size distributions (polydisperse systems)

When the arrangement of the bubbles in the medium is random (not periodic) and bubbles are well separated, light scattered by each bubble is considered to be incoherent, and the angular distribution of light scattered by those bubbles is calculated as the sum of the light intensity scattered by each bubble.

Fig. 4 shows distributions of bubbles we assumed in the model, and Fig 5. shows the corresponding expected angular distributions of scattered light.

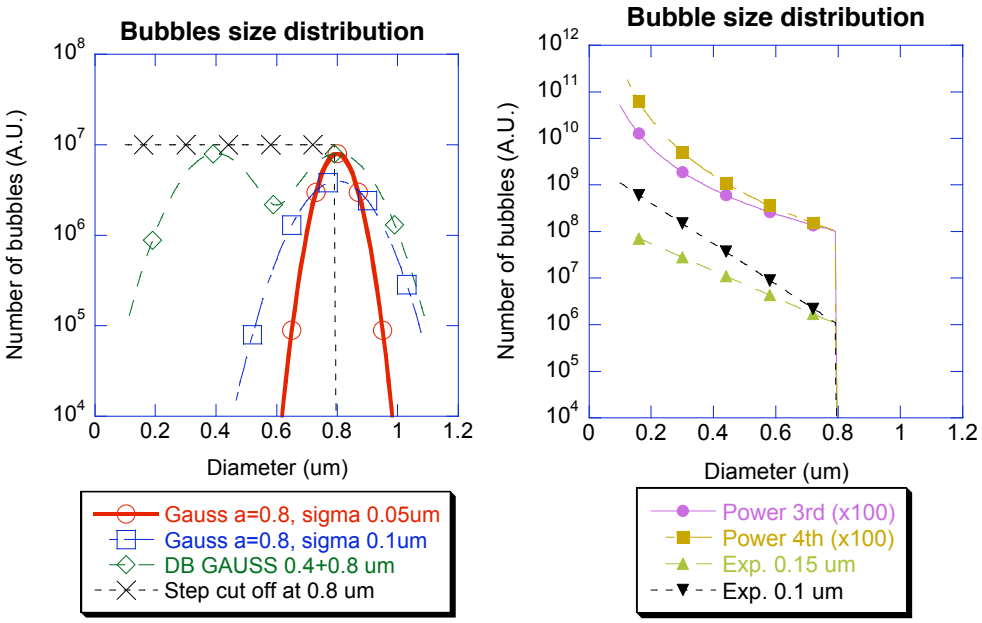

Fig. 4 Distributions of bubbles we assumed in the model. The power low curves (population scales inversely proportional to 3rd or 4th order of the bubble size) were multiplied by 100 for better visibility.

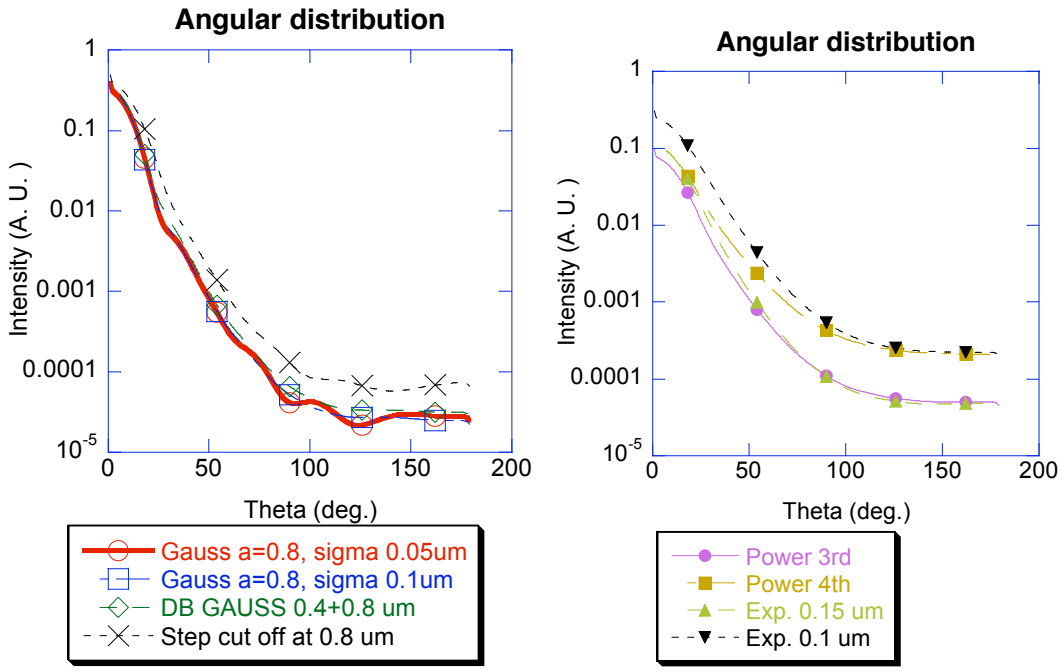

Fig. 5 Expected angular distribution of Mie scattering

The distributions and results are:

(1) Gaussian distribution, mean diameter 0.8 μm, st. dev. 0.05 μm.
The angular distribution is almost identical to that expected from a uniform void diameter of 0.8 μm. The angular distribution has darker bands corresponding to mean diameter of the bubbles.

(2) Gaussian distribution, mean diameter 0.8 μm, st. dev. 0.1 μm.
The angular profile is similar to (1), but the dark bands are more smoothed due to the overlapping of light scattered by different diameter bubbles. Even this narrow distribution width is sufficient to smooth out the bubble size information included in the dark band structure.

(3) Step function, cutoff at 0.8 μm.
Since the cross section of Mie scattering is a strong function of the bubble size, the Mie scattering signal from the largest bumps (cut off around 0.8 μm) dominates the signal. The overall shape is similar to (2) because smaller bubbles are not contributing to the detected signal.

(4) Double Gaussian, mean diameter 0.4 μm and 0.8 μm.
The Mie scattering signal from 0.8 μm bubbles is dominating the results. The Mie scattering signal from 0.4 μm bubbles are not contributing significantly to the scattering.

(5) Power law, 3^{rd} order, cutoff 0.8 μm.

The angular distribution has no dark bands or distinctive features. All dips and peaks are smoothed out.

(6) Power law, 4^{th} order, cutoff 0.8 μm.
As in (5), the profile has no dips or peaks. However, compared with (5), it appears that the contrast of forward and backward scattering could be used to infer the index of the power law.

(7) Exponential, slope 1/e every 0.15 μm, cutoff 0.8 um.
The results are similar to (5) but with more backscattering.

(8) Exponential, slope 1/e every 0.1 μm, cutoff 0.8 μm
Compared to (7), this profile has more backscattering.

Conclusion
The angular distribution of scattered light may provide a rough idea of the bubble size population. Larger bubbles in the Mie scattering region give more forward scattering. For smaller bubbles, light is scattered by Rayleigh scattering which has a more uniform angular distribution.

V. Spectrum of light scattered by bubbles at a fixed angle.

(A) Observation of forward scattering from 30 degrees

Fig. 6. shows the spectrum of scattered light observed from 30 degrees with respect to the direction of illumination, for the same bubble size distribution functions considered above.

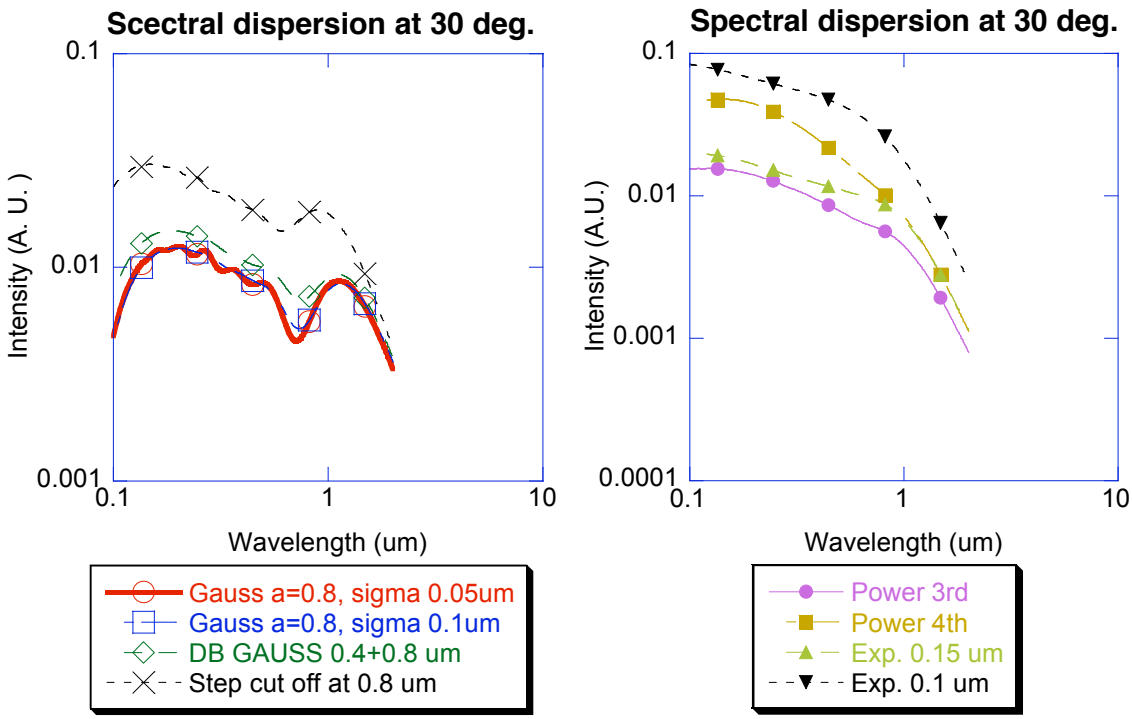

Fig 6. Spectrum white light scattered at 30 degrees.

(1) Gaussian distribution, mean diameter 0.8 μm, st. dev. 0.05 μm.
The expected spectrum is almost identical to that expected from uniform 0.8 μm bubbles. It has resonance structures corresponding to the most probable bubble size.

(2) Gaussian distribution, mean diameter 0.8 μm, st. dev. 0.1 μm.
The spectrum is similar to (1), but resonances on the shorter wavelength side are smoothed out.

(3) Step function, cutoff at 0.8 μm.
The result is almost identical to that of (1) and (2), because the largest bubbles around the cutoff (0.8 μm) are dominating the signal.

(4) Double Gaussian, mean diameters 0.4 μm and 0.8 μm.
The signal from 0.8 μm bubble is dominating the results. The scattering from 0.4 μm bubbles is not significant.

(5) and (6) Power law, 3rd and 4th order, cutoff 0.8 μm.
The slope of the spectrum (or "color temperature") of the scattered light has some dependence on the index of the power law of the bubble distribution. The steeper the distribution, the higher the "color temperature".

(7) and (8) Exponential distributions with slope 1/e every 0.15 and 0.1 μm.

The results are similar to (6) and (7), but with less scattering at short wavelengths because of fewer bubbles with diameters smaller 0.3 μm. These results suggesting that it may possible to distinguish between bubble distributions (7) and (8) by spectroscopy of scattered white light.

(B) Spectrum vs. maximum bubble size

We also set the cutoff diameter smaller (0.4 μm instead of 0.8 μm) as a test of the sensitivity of the spectra to the cutoff diameter.

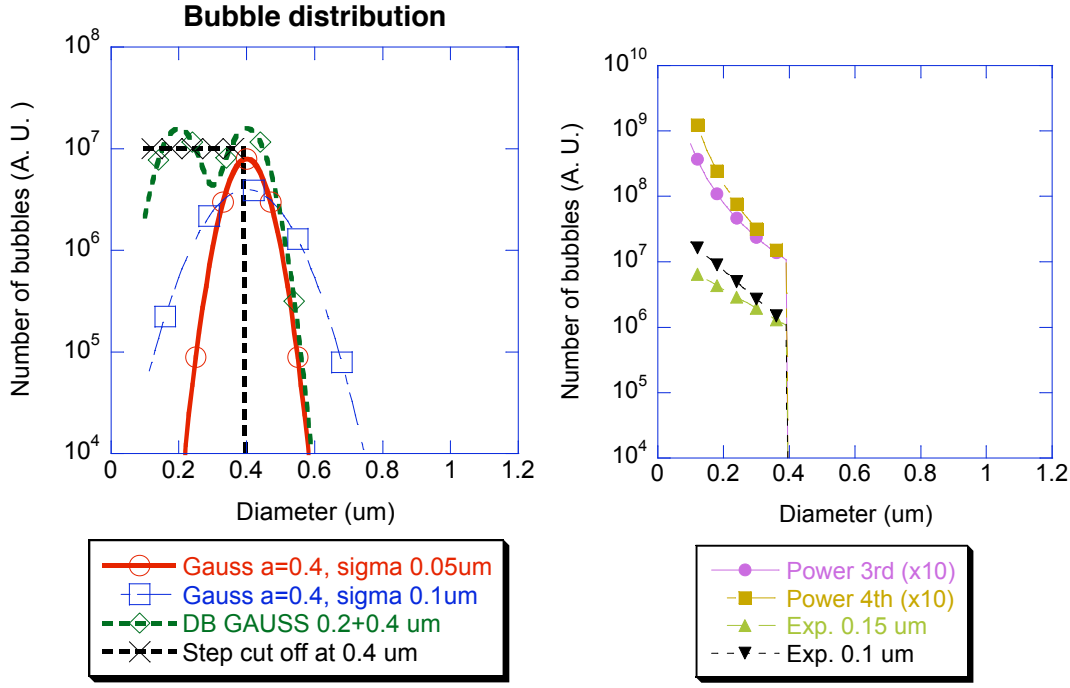

Fig. 7. Cutoff of the bubble distribution was set to 0.4μm.

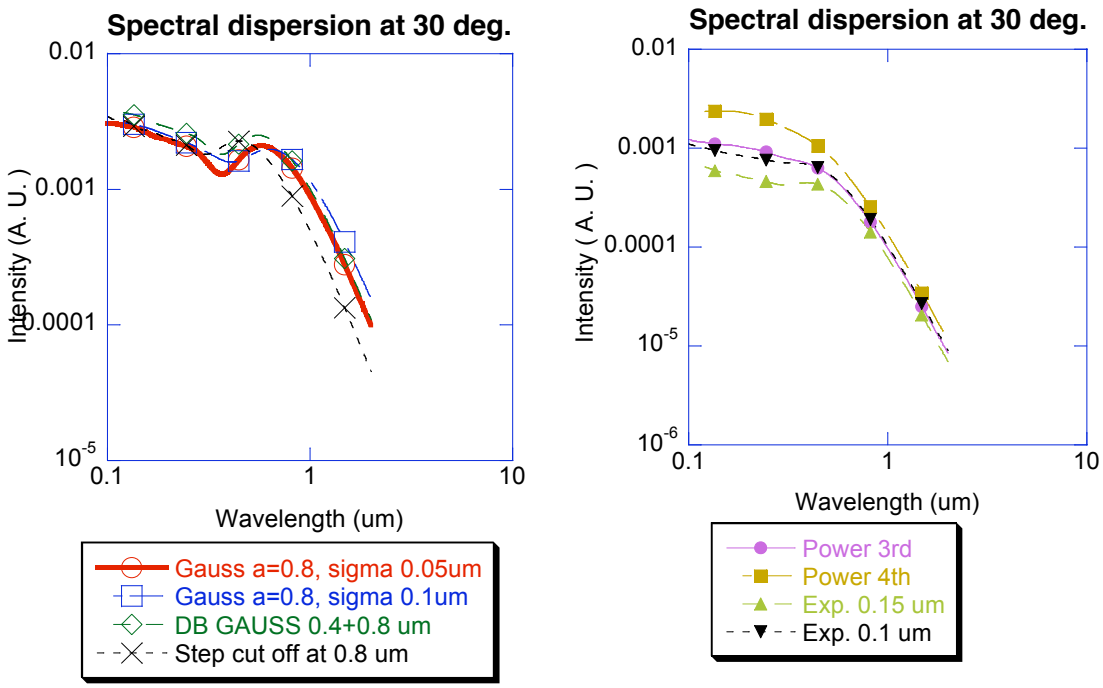

Fig. 8. Maximum bubble size vs. expected spectra of scattered light.

As expected, spectral features similar to (A) were observed, but with everything shifted to lower wavelengths. The relatively gradual slope in the shorter wavelength region is Mie scattering. If the bubble distribution is monodisperse, the scattered light spectrum has a large resonance peak approximately at the diameter of the bubble. When the wavelength is longer than the cutoff of the bubble diameter distribution (0.4μm), Rayleigh scattering is dominating, and the intensity of the scattered light is scaling approximately as the inverse 4th power of the wavelength.

(C) Observation of back scattering from 150 degrees

In order to check how the spectra of scattered light responds to the bubble size distribution, back scattering towards θ = 150 degrees was calculated. Figure 9 shows the result. The spectrum of backscattered lights has very little wavelength dependence, like light scattering by a *"white cloud"*, and the response is almost independent of the bubble distribution. Therefore, spectral measurements of back scattering are not useful for measuring bubble size distributions.

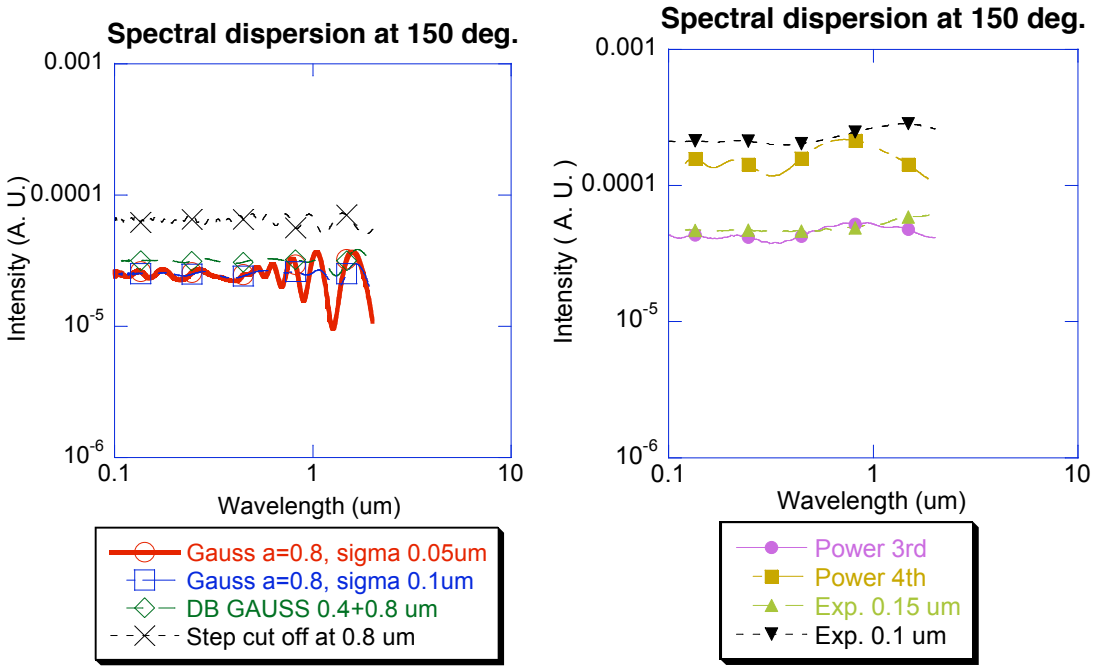

Figure 9. Calculated spectra of light scattered to 150 degrees.

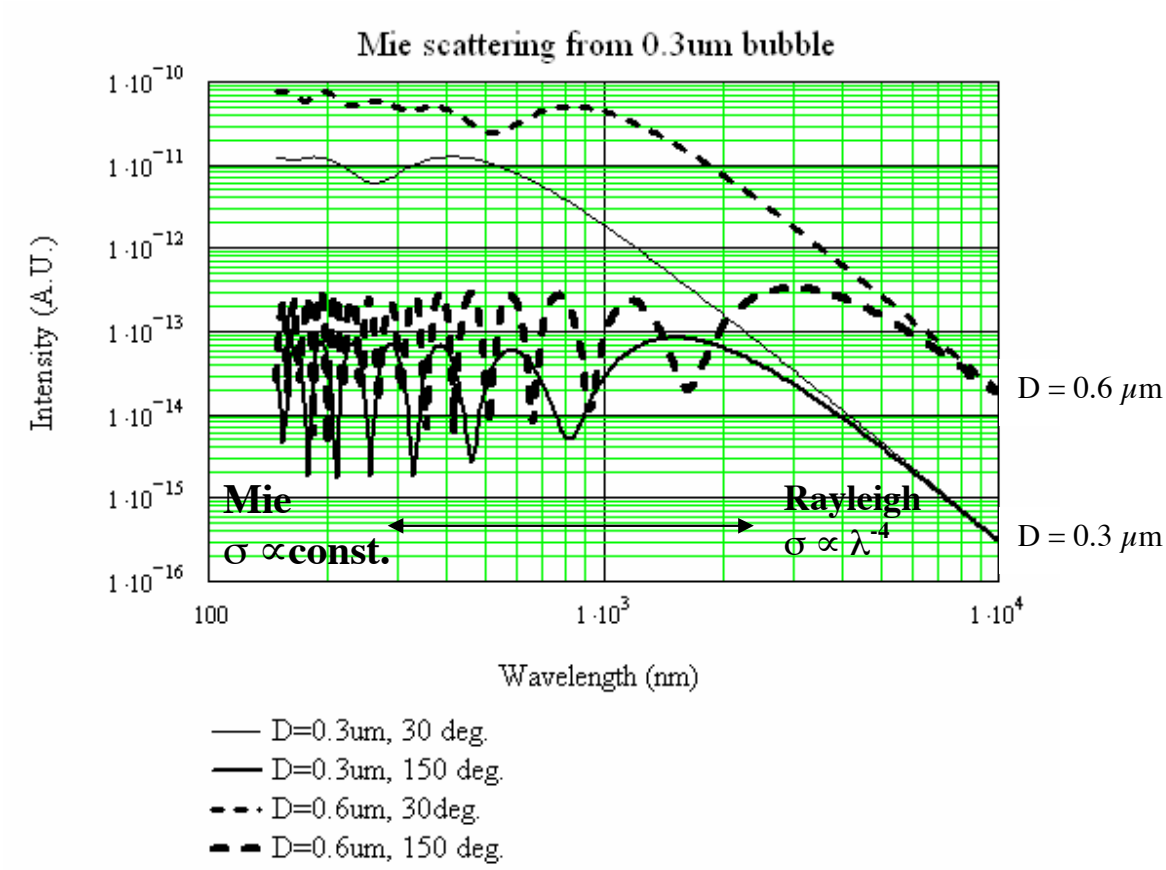

Figure 10. Spectra of white light scattered by 0.3 μm and 0.6 μm bubbles toward 30 and 150 degrees.

This phenomenon is shown more clearly in Fig. 10. The forward scattering has a clear transition between Mie scattering in visible wavelength region (scattering cross-section σ is independent of wavelength) and Rayleigh scattering ($\sigma \propto \lambda^{-4}$). The modulation in cross section can be observed if the sample has uniform bubble sizes. If the bubble size distribution has finite width, this modulation will be smoothed out. However, the large structure of forward scattering (transition between Mie and Rayleigh scattering) will not be smoothed out. Therefore, the spectrum of forward scattering can provide information on the population of bubble sizes even though the accuracy is limited by the sharpness of the transition between Mie scattering and Rayleigh scattering.

VI. CONCLUSION

I studied feasibility of the static light scattering method for size distribution measurement of ^{3}He bubbles in DT ice layer. The static light scattering method is aiming to infer the size distribution of bubbles in dielectric medium by analyzing angular distribution or spectral dispersion of lights scattered by bubbles.

When all the bubbles have the same radius (i.e. monodisperse), in angular or spectral distribution of scattered light has many microscopic structures (peaks and dips) which is characteristic to the bubble size. Then position of those dips and peaks in observed scattered light can be used to infer the bubble size. If the bubble size has finite distribution (i.e. polydisperse), those microscopic structure are smoothed out and can not be used for bubble size distribution measurement.

The distribution of ^{3}He bubbles in DT ice layer is considered to be polydisperse. Therefore it is not possible to measure the bubble size distribution from the microscopic feature of scattered light.

However, even microscopic features are smoothed out, the spectral distribution of the scattered light still has distinguishable macroscopic transition between Mie scattering region (the scattering cross-section σ independent to the wavelength) and Rayleigh scattering region ($\sigma \propto \lambda^{-4}$). With using this transition, it is possible to roughly infer the distribution of bubbles. As shown in Fig. 6 and Fig 8, the spectrum of scattered light observed from 30degree showed different spectra for different bubble distribution even in polydisperse case.

Since the transition between Mie and Rayleigh scattering is gradual, expected measurement accuracy of bubble diameter is limited. This method is not sensitive to small difference nor distortion of bubble size distribution.(like peaks / valleys on broad distribution function).

The scattered light signal can be dominated by light scattering from interrogated ice volume. Therefore, existence of sparse but large bubble can strongly affect the result.

Considering those drawbacks, I conclude that this static light scattering method can be useful for relative measurement of the bubble distribution when the distribution curve is reproducible and well characterized. For example, a temporal growth of bubble size distribution or relative comparison of bubble densities in different samples can be done with this method.

If the bubble size distribution is unknown or the distribution is not reproducible, interpretation of data can be complicated and this method will not provide quantitative information.

ACKNOWLEDGEMENT

This work was performed under the auspices of the U.S. Department of Energy by the University of California, Lawrence Livermore National Laboratory under contract No. W-7405-Eng-48.

REFERENCES

[1] M. Born and E. Wolf, "Principles of Optics", 7th (expanded) edition, Cambridge University Press, Cambridge, 1999, p.759

[2] For example,
B.J. Berne, and R. pecora, Dynamic Light Scattering (Robert E. Krieger publishing company Malabar, Florida 1990): W. Brown, Dynamic Light Scattering the method and some applications, (Clarendon Press, Oxford 1993).

[3] M. Born and E. Wolf, "Principles of Optics", 7th (expanded) edition, Cambridge University Press, Cambridge, 1999, pp.770-772.